Available online at www.sciencedirect.com
SCIENCE DIRECT®
Bioorganic & Medicinal Chemistry Letters 15 (2005) 1045–1050
Bioorganic & Medicinal Chemistry Letters

Conformational analysis of rhazinilam and three-dimensional quantitative structure–activity relationships of rhazinilam analogues

Hiroshi Morita,[a,*] Khalijah Awang,[b] A. Hamid A. Hadi,[b] Koichi Takeya,[c] Hideji Itokawa[c] and Jun'ichi Kobayashi[a]

[a]*Graduate School of Pharmaceutical Sciences, Hokkaido University, Sapporo 060-0812, Japan*
[b]*Department of Chemistry, University of Malaya, 59100 Kuala Lumpur, Malaysia*
[c]*Department of Pharmacognosy, School of Pharmacy, Tokyo University of Pharmacy & Life Science, 1432-1 Horinouchi, Hachioji, Tokyo 192-03, Japan*

Received 11 November 2004; revised 9 December 2004; accepted 10 December 2004
Available online 12 January 2005

Abstract—3D QSAR of rhazinilam (**1**), an alkaloid isolated from *Rhazya stricta* (Apocynaceae) with an activity involving disassembly of microtubules and its derivatives was investigated by using the comparative molecular field analysis (CoMFA). In an effort to get a better understanding of the correlation between conformation and antitubulin activity of **1**, most probable minimum energy conformation in solution of **1** was analyzed on the basis of NMR data of **1** in solution. The results indicated a correlation between the antitubulin activity of these alkaloids and the steric and electrostatic factors, which modulate their biological activity, and accounted for the potent activities of **1** with suitable relationship for the overall conformation.

1. Introduction

Rhazinilam (**1**),[1] an indole secoalkaloid related to the aspidospermane group, has been isolated from different Apocynaceae species, and inhibits disassembly of microtubule. It is also considered as the leading compound in cancer chemotherapy.[2] The mechanism of the action of **1** is a unique one involving disassembly of microtubules.[2] A preliminary structure–activity relationship (SAR) study has indicated that the two aromatic rings and the lactam carbonyl group at C-2 were essential features for activity.[3] More precise SAR studies indicated that the electronic properties of the aromatic rings, such as the electronic distribution of the pyrrole ring and its aromaticity, were important for the binding to tubulin.[4] In addition, various factors such as the absolute configuration, the overall conformation, steric hindrance, and hydrophobic effect were shown to be of crucial importance to show activity.[5]

In order to get a better understanding of the correlation between conformation and antitubulin activity of rhazinilam (**1**), we investigated most probable minimum energy conformation in solution of **1** and three-dimensional quantitative structure–activity relationship (3D-QSAR) by using comparative molecular field analysis[6] (CoMFA).

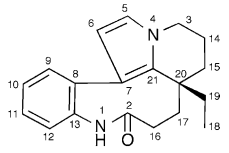

rhazinilam (**1**)

2. NMR assignments

To determine the solution conformation of rhazinilam (**1**), complete assignments of the ^{1}H and ^{13}C signals in $CDCl_3$ and CD_3OD were made by 2D NMR experiments such as ^{1}H–^{1}H COSY, HOHAHA, HMQC, and HMBC (Table 1). Since each of the magnetic non-equivalent methylene protons could be assigned, nine membered ring in **1** may retain some stable backbone conformation

Keywords: 3D QSAR; CoMFA; Rhazinilam; Antitubulin activity.
* Corresponding author. Tel.: +81 11 7064985; fax: +81 11 7064989; e-mail: jkobay@pharm.hokudai.ac.jp

0960-894X/$ - see front matter © 2004 Elsevier Ltd. All rights reserved.
doi:10.1016/j.bmcl.2004.12.027

Table 1. ^{1}H and ^{13}C NMR data of rhazinilam (**1**) in $CDCl_3$ and CD_3OD at 300 K

Position	δ_H [int. mult, J (Hz)][a]	δ_H [int. mult, J (Hz)][b]	δ_C[a]	δ_C[b]
NH	6.95 (1H, br s)	7.91 (1H, s)		
2			177.9	180.0
3*R*	3.79 (1H, dt, 4.8, 12.1)	3.79 (1H, ddd, 4.6, 12.2, 12.2)	46.1	47.1
3*S*	4.02 (1H, br dd, 5.3, 12.1)	4.03 (1H, br dd, 5.2, 12.2)		
5	6.51 (1H, d, 2.7)	6.53 (1H, d, 2.7)[c]	119.3	[d]
6	5.76 (1H, d, 2.7)	5.72 (1H, d, 2.7)[c]	109.6	[d]
7			117.2	118.7
8			140.3	141.4
9	7.43 (1H, dd, 1.8, 7.5)	7.40 (1H, dd, 1.5, 7.5)	131.5	132.5
10	7.31 (1H, ddd, 1.8, 7.5, 7.5)	7.32 (1H, ddd, 1.5, 7.5, 7.5)	127.5	128.1
11	7.35 (1H, ddd, 1.8, 7.5, 7.5)	7.38 (1H, ddd, 1.5, 7.5, 7.5)	128.1	129.1
12	7.21 (1H, dd, 1.8, 7.5)	7.22 (1H, dd, 1.5, 7.5)	126.7	127.5
13			137.7	139.7
14*R*	2.23 (1H, dddd, 3.2, 5.6, 13.4, 26.0)	2.21 (1H, dddd, 3.2, 5.5, 13.4, 25.9)	19.5	20.7
14*S*	1.86 (1H, m)	1.90 (1H, m)		
15*R*	1.72 (1H, dt, 3.2, 13.4)	1.79 (1H, ddd, 3.2, 13.4, 13.4)	33.1	34.4
15*S*	1.55 (1H, ddd, 3.2, 3.2, 13.4)	1.54 (1H, ddd, 3.2, 3.2, 13.4)		
16*R*	2.39 (1H, t, 13.0)	2.34 (1H, t, 10.0)	28.0	29.2
16*S*	1.99 (1H, dd, 8.0, 13.0)	1.91 (1H, m)		
17*R*	2.46 (1H, t, 13.0)	2.45 (1H, t, 10.0)	36.6	38.0
17*S*	1.49 (1H, dd, 8.0, 13.0)	1.52 (1H, m)		
18	0.72 (3H, t, 7.4)	0.73 (1H, t, 7.4)	8.2	8.5
19*R*	1.24 (1H, m)	1.24 (1H, m)	30.1	31.2
19*S*	1.46 (1H, m)	1.50 (1H, m)		
20			38.9	40.2
21			130.5	131.2

[a] In $CDCl_3$.
[b] In CD_3OD.
[c] Data measured in CD_3OH; *R* and *S* represent pro-*R* and pro-*S*, respectively.
[d] Not observed in CD_3OD because of D–H exchange.

in solution. Electron-donating substituents of pyrrole ring are known to increase the rate of hydrogen exchange,[7] that has been studied by isotope exchange.[8] In CD_3OD, ^{1}H and ^{13}C signals at C-5 and C–6 in **1** were not observed by deuterium exchange. The trisubstituted pyrrole ring in **1** appeared to be the first example in pyrrole system where proton exchange at C-5 and C-6 was sufficiently fast on the NMR time scale to observe its effects by ^{1}H NMR (CD_3OD) under neutral conditions.[9]

3. Conformational analysis

Structure optimization was performed by using the systematic pseudo Monte Carlo (MC) search,[10] in the MacroModel (version 5.0) on an IRIS 4D computer in vacuo. Each conformation generated by each MC calculation (3000 step) was minimized by the use of molecular mechanics calculation of MMFF force field[11] to reduce the gradient rms to less than 0.001 kcal/Å mol with a distance-dependent dielectric, $\varepsilon = R_{ij}$. To eliminate possible duplicate conformations, comparison was performed on the heavy atoms only. The extended cutoff distances employed were 8 Å for van der Waals, 20 Å for charge/electrostatics, and 10 Å for charge/multipole electrostatics. The global minimum conformation of **1** was selected by the clustering analysis and furthermore optimized by semiempirical PM3 calculation.[12]

On the other hand, to compare with that of the above calculated conformer, the interatomic distances of the rhazinilam (**1**) were calculated by the program TRIAD in SYBYL[13] using the integrated volumes of NOE correlations in the phase sensitive NOESY spectrum in $CDCl_3$. These conformational characteristics of **1** implied by the MC search followed by PM3 calculation were compatible with those observed in the crystal conformation of **1** by X-ray analysis[1] (Table 2). Judging from the interatomic distances in Table 2 and superimposed structures (Fig. 1), the overall conformation of **1** in solution was also similar to that in the crystal structure, although there were some violations.[1]

3.1. Rhazinilam (1) and its analogues (2–39)

Rhazinilam (**1**) used in this experiment was prepared as described previously[4] and the biological data of rhazinilam analogues (**2**–**39**) were obtained from the literatures,[5] though inactive analogues were not included for QSAR analysis.

4. CoMFA analysis[6]

CoMFA was initiated by using the minimum-energy conformations obtained as described above. The default SYBYL settings were used unless otherwise noted. Stable conformers of **2**–**39** as shown in Figure 3 were aligned via root mean square (rms) fitting of backbone atoms, C-8 to C-13, to the corresponding atoms of rhazinilam (**1**) chosen as the template molecule.

Table 2. Distances (Å) between the protons of rhazinilam (**1**)

Protons		X-ray[a]	PM3[b]	NOE[c]
H9	H10	2.46	2.49	2.8
H10	H11	2.45	2.49	3.1
NH	H12	2.73	2.89	3.3
H6	H9	3.69	3.51	3.5
NH	H6	3.87	3.93	4.3
H12	H16*R*	3.75	3.62	3.4
H19*R*	H9	3.05	2.90	2.9
H19*S*	H9	4.53	3.10	3.2
H18	H9	3.13	5.12	4.4
H5	H6	2.69	2.72	2.9
H3*S*	H5	2.66	2.74	2.7
H3*R*	H5	3.17	3.04	3.1
H3*S*	H14*R*	2.46	2.46	2.5
H3*R*	H14*S*	2.46	2.44	2.5
H3*R*	H15*R*	2.54	2.66	2.6
H14*R*	H17*R*	2.14	1.88	2.2
H16*S*	H17*R*	2.63	2.73	2.2
H14*R*	H15*S*	2.53	2.53	2.6
H14*S*	H15*R*	2.52	2.57	2.6
H14*S*	H15*S*	2.50	2.45	2.6
H19	H15*R*	2.89	2.55	2.6
H19*R*	H15*S*	3.81	3.80	3.3
H19*S*	H15*S*	2.59	3.35	2.9
H18	H15*R*	2.73	3.32	3.9
H3*S*	H14*S*	2.57	2.59	2.7

[a] Distances from X-ray structure.
[b] Distances from structure optimized by PM3 calculation after MC simulation.
[c] Distances calculated by NOE integral intensities.

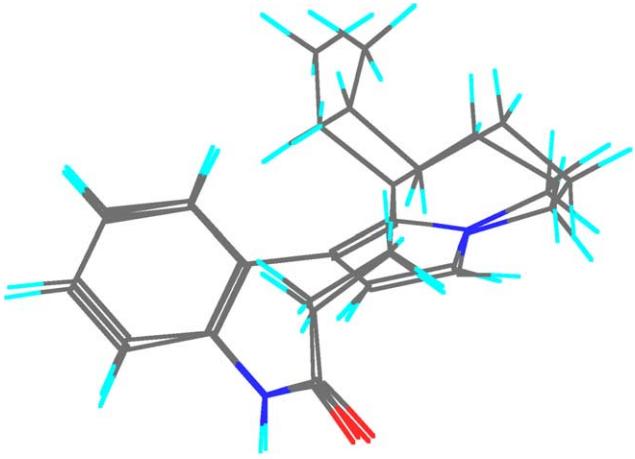

Figure 1. Superimposed structures of rhazinilam (**1**) obtained by X-ray analysis and PM3 calculation.

For each of the alignment sets, the steric and Coulombic potential energy fields were individually calculated at each lattice intersection of a regularly spaced grid of 2.0 Å units in all *x*, *y*, and *z* directions. The steric terms represent the van der Waals interactions, whereas the Coulombic terms represent the electrostatic interactions for which a distance-dependent dielectric expression $\varepsilon = R_{ij}$ was adopted. The grid pattern was generated automatically by the SYBYL/CoMFA routine. An sp^3 carbon atom with a +1.0 charge was selected as a probe for the calculation of the steric and electrostatic field. Values of the steric and electrostatic energies were truncated at 30 kcal/mol.

To obtain a 3D-QSAR, partial least squares (PLS) fitting was used. The PLS method has been applied to rationalize those structural features affecting the biological activity. The PLS algorithm was initially used with the cross-validation option to obtain the optimal number of components needed for the subsequent analysis of the data. In the leave-one-out cross-validation, each compound was systematically excluded from the set and its activity predicted by a model derived from the rest of the compounds. The optimal number of components ($n = 5$) was then chosen so that it would yield either the smallest rms error or the largest cross-validated r^2 value. A final PLS analysis was then performed by using the reported optimum number of components, with no cross-validation. This generated a fitted correlation of the entire training set with conventional r^2 values. The steric and electrostatic fields were scaled according to the CoMFA standard deviations in order to give them the same potential weights on the resulting QSAR. The 3D-QSAR calibration model was then employed to predict the inhibitory values of some rhazinilam analogues in the test set, after conformational analysis and alignments were performed by the method as indicated above.

The results of the CoMFA analysis are summarized in Table 3, and evidence for the reliability of estimate by the CoMFA-derived model is provided in Figure 4, which shows plots of actual versus predicted inhibition of disassembly of microtubule [$\log(1/IC_{50})$]. It is evident that the CoMFA-derived QSAR gave good cross-validated r^2, thereby indicating a considerably reliable capacity of this method for predicting the inhibition of disassembly of microtubule. The relative contribution of the steric field to this model was larger than that of the electrostatic one.

The major steric and electrostatic features of the QSAR are represented in Figure 5 in the form of three-dimensional contour maps, displayed as transparent surfaces. The surfaces at the top of Figure 5 indicate the areas in space around the template molecule (**1**) whose increases (green region) and/or decreases (yellow region) in the steric bulk could enhance the inhibition of disassembly of microtubule. Contour maps of the electrostatic field contributions are provided in Figure 5 (below).

In the steric CoMFA map, the side chain at C-20 would enhance the inhibition of disassembly of microtubule. This is consistent with the hypothesis of the hydrophobic interaction with tubulin at this position;[5b] in addition that at C-5 of pyrrole ring would enhance the activity. On the other hand, this map also indicated that smaller bulks at amide nitrogen atom and aromatic ring would also enhance the activity. Previous studies also indicate that the lactam site is an important feature because it is probably directly involved in binding of tubulin.[4] Effect of the steric hindrance on ring A (Fig. 2) for the inhibition of disassembly of microtuble agrees with

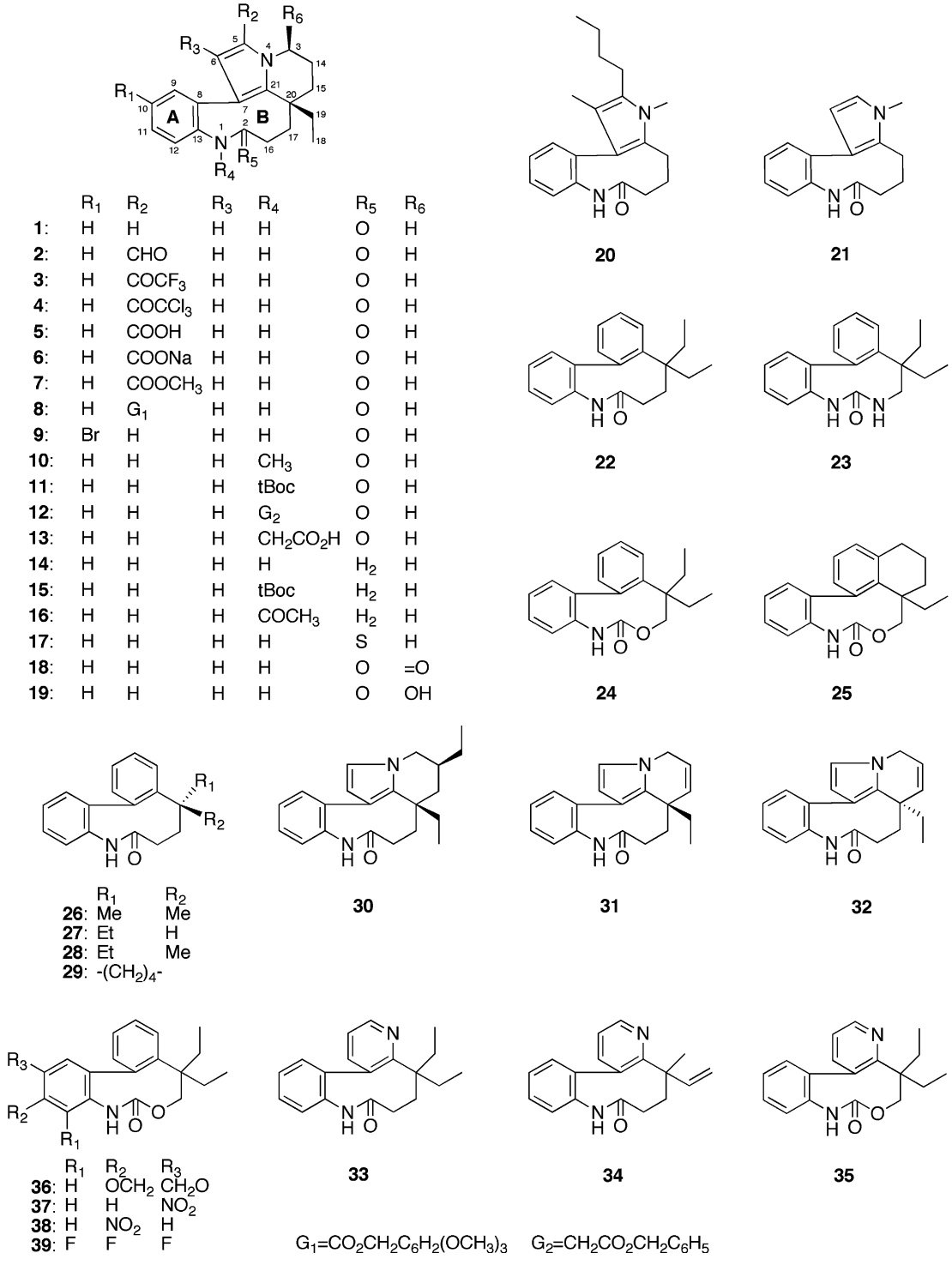

Figure 2. Structures of rhazinilam (**1**) and its analogous (**2**–**39**) used for CoMFA analysis.

recent study by Baudoin et al. that the increase of the steric hindrance on ring A induced by the addition of substituents was harmful to the antitubulin activity.[5e] In the electrostatic CoMFA map, the regions where a more positive electrostatic interaction would improve the inhibition of disassembly are located around the aromatic ring and amide bond, whereas, negative electrostatic interactions are located between C-16 and aromatic ring. Pasquinet et al. mentioned that the charge distribution was important for the activity by synthesis of tricyclic hindered phenylpyridine lactams in place of the phenylpyrrole lactams.[5f] The dihedral angles of the biary moiety have been known to play an essential role in the inhibition of microtubule disassembly.[5d] It appears that the conformation of ring B (Fig. 2) of the molecule merely serves to hold the dihedral angles of the biaryl moiety in the active shape (ca. 90°) for binding to tubulin.

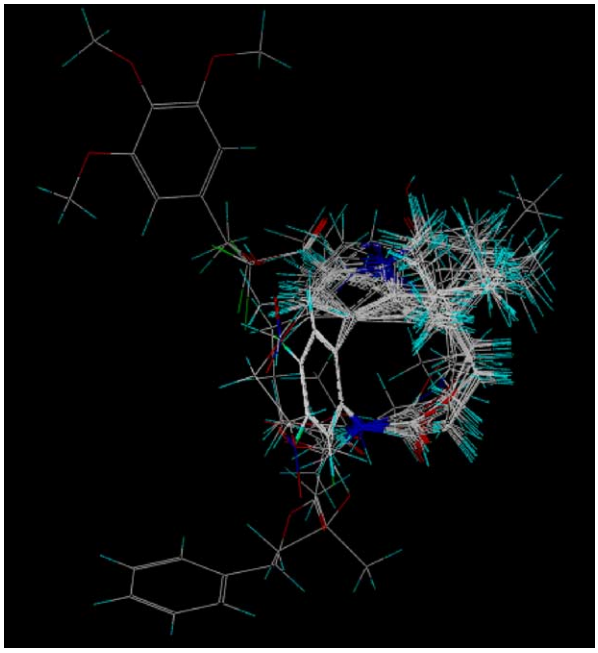

Figure 3. Superimposed structures of rhazinilam (**1**) and its analogues (**2**–**39**).

Table 3. Summary of CoMFA-PLS results

Opt. no of components	5
Probe atom	c (sp^3, +1)
Cross-validated r^2	0.582
Std error of estimate	0.253
r^2	0.877
F values ($n1 = 5$, $n2 = 29$)	47.066
Contributions	
Steric	0.574
Electrostatic	0.426

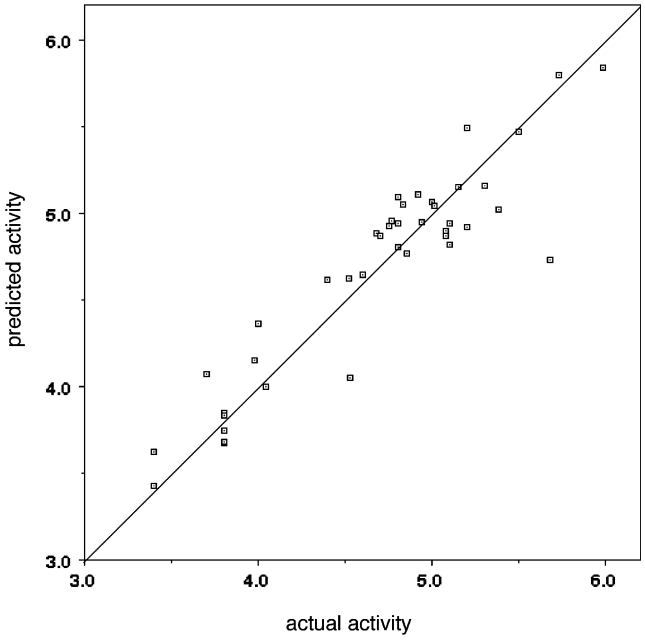

Figure 4. Plot of actual versus predicted inhibitory activities of disassembly of microtuble ($r^2 = 0.877$). The activities are expressed by log $1/IC_{50}$.

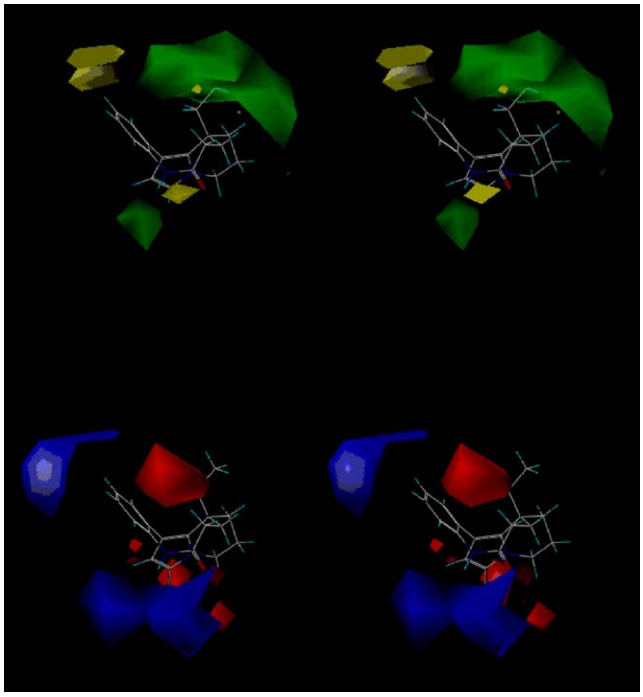

Figure 5. Stereoview of the CoMFA contour plot from the PLS analysis. Above: steric, below: electrostatic. Regions where increased steric bulk is associated with enhanced activity are indicated in green, whereas regions where increased steric bulk is associated with diminished activity are indicated in yellow. On the other hand, regions where increased positive charge is favorable for activity are indicated in blue, whereas regions where increased negative charge is favorable are indicated in red.

This CoMFA model derived from the above rhazinilam analogues has not been used to calculate the new derivatives, but the present model can be generally used for estimation of the activities of active derivatives because it has a high cross-validated r^2 and r^2. Thus, the CoMFA results have been applied successfully to rationalize the inhibitory activities of tubulin disassembly of rhazinilam (**1**) and its analogues (**2**–**39**) in terms of their steric and electrostatic properties, and it became clear that similar correlation may be observed in the previous papers separately.[5] It is distinctly possible that a combination of various substituents and conformation of the whole molecule may effect potency of inhibition of tubulin disassembly. Estimation of biological action by the use of CoMFA derived models may be improved if more substituents are taken into calculation.

Acknowledgements

This work was partly supported by a Grant-in-Aid from the Ministry of Education, Science, Sports, and Culture of Japan.

References and notes

1. Abraham, D. J.; Rosenstein, R. D.; Lyon, R. L.; Fong, H. H. S. *Tetrahedron Lett.* **1972**, 909–912.

2. Thoison, O.; Guénard, D.; Sevenet, T.; Kan-Fan, C.; Quirion, J. C.; Husson, J. P.; Deverre, J. R.; Chan, K. C.; Potier, P. *C. R. Acad. Sc., Paris II* **1987**, *304*, 157.
3. Alazard, J.-P.; Millet-Paillusson, C.; Boye, O.; Guénard, D.; Chiaroni, A.; Riche, C.; Thal, C. *Bioorg. Med. Chem. Lett.* **1991**, *1*, 725–728.
4. David, B.; Sevenet, T.; Thoison, O.; Awang, K.; Pais, M.; Wright, M.; Guénard, D. *Bioorg. Med. Chem. Lett.* **1997**, *7*, 2155–2158.
5. (a) Pascal, C.; Dubois, J.; Guénard, D.; Tchertanov, L.; Thoret, S.; Guéritte, F. *Tetrahedron* **1998**, *54*, 14737–14756; (b) Pascal, C.; Dubois, J.; Guénard, D.; Guéritte, F. *J. Org. Chem.* **1998**, *63*, 6414–6420; (c) Dupont, C.; Guénard, D.; Tchertanow, L.; Thoret, S.; Guéritte, F. *Bioorg. Med. Chem.* **1999**, *7*, 2961–2969; (d) Dupont, C.; Guénard, D.; Thal, C.; Thoret, S.; Guéritte, F. *Tetrahedron Lett.* **2000**, *41*, 5853–5856; (e) Baudoin, O.; Claveau, F.; Thoret, S.; Herrbach, A.; Guénard, D.; Guéritte, F. *Bioorg. Med. Chem.* **2002**, *10*, 3395–3400; (f) Pasquinet, E.; Rocca, P.; Richalot, S.; Guéritte, F.; Guénard, D.; Godard, A.; Marsais, F.; Queguiner, G. *J. Org. Chem.* **2001**, *66*, 2654–2661.
6. Cramer, R. D., III; Patterson, D. E.; Bunce, J. D. *J. Am. Chem. Soc.* **1988**, *110*, 5959–5967.
7. Almerico, A. M.; Cirrincione, G.; Diana, P.; Grimaudo, S.; Dattolo, G.; Aiello, E.; Mingoia, F. *J. Heterocycl. Chem.* **1995**, *32*, 985–989.
8. Bean, G. P.; Wilkinson, T. J. *J. Chem. Soc., Perkin Trans. 2* **1978**, 72–77.
9. Rosa, M. D.; Issac, R. P.; Houghton, G. *Tetrahedron Lett.* **1995**, *36*, 9261.
10. Goodmann, J. M.; Still, W. C. *J. Comput. Chem.* **1991**, *12*, 1110–1117.
11. Halgren, T. *J. Am. Chem. Soc.* **1990**, *112*, 4710–4723.
12. Stewart, J. J. P. *J. Comput. Chem.* **1989**, *10*, 221–264.
13. Molecular modeling software SYBYL 6.5 on an O2 Workstation (Silicon Graphics).